Journal of Geophysics and Engineering 2009, vol.6, pp.21–28
doi:10.1088/1742-2132/6/1/002

Seismic resolution enhancement for tight-sand gas reservoir characterization

Qigang Gan[1], Duo Xu[1], Jianming Tang[1] and YanghuaWang[2]

1 Research Institute of Exploration and Development, Southwest Petroleum Company of Sinopec, Deyang City, Sichuan Province 618000, People's Republic of China
2 Centre for Reservoir Geophysics, Department of Earth Science and Engineering, Imperial College London SW7 2BP, UK

Abstract

This is a case study on the application of inverse-*Q* filtering to improve the resolution of 3D seismic data, for the characterization of tight-sand gas reservoirs. When seismic waves propagate through multiple tight-sand layers in the subsurface media, the energy of high-frequency components is absorbed, and the wavelet shape is distorted. Stabilized inverse-*Q* filtering is able to simultaneously compensate the amplitude and correct the phase of seismic waveforms. After application to 3D seismic data, the frequency bandwidth has been increased by about 10 Hz, and the width of the wavelet has been narrowed, so that we are able to identify reflections of thin sand layers clearly. Due to the phase correction in inverse-*Q* filtering, filtered seismic traces can match the synthetic traces at well locations. Because of the high signal-to-noise ratio with the stabilization scheme, low-amplitude zones of interest corresponding to target high-fracture areas can be easily identified, and the detail within the anomalies can also be observed. Finally, spatial variations of tight-sand layers are depicted in the inversion profile with high resolution.

Keywords: high-resolution seismic, hydrocarbon detection, inverse-*Q* filtering, reservoir characterization, resolution enhancement

1. Introduction

This is a case study on the resolution enhancement of three-dimensional (3D) seismic data. The exploration and production target is a series of tight-sand gas reservoirs at depths between 3000 and 4600 m. We use the stabilized inverse-*Q* filtering algorithm (Wang, 2008) to improve the resolution of the 3D seismic data cube, and then analyse the seismic signals around the target gas reservoirs.

The study area is located in the west Sichuan basin, between the Longmen Mountains and Longquan Mountains, southwestern China (Figures 1a and 1b). The hydrocarbon exploration target is mainly the gas reservoirs existing within tight sands (Figure 1c). Because the gas reservoirs are in tight clastic sediments with the following influential factors: deep traps (3000-4600 m in depth), tight rocks (porosity less than 4%), strong heterogeneity, variety of reservoir types (porous and/or fractured) and complex gas-water contacts (Tang et al., 2008), there are three major challenges presented in the exploration and production of deep gas reservoirs: the characterisation of reservoir distribution, prediction of fracture zones in reservoirs, and estimation of potential gas contents.

When seismic waves propagate through the subsurface anelastic media, the energy of high-

frequency plane-wave components is absorbed and, due to the velocity dispersion of different frequencies, the wavelet shape is also distorted. This anelastic characteristic of the media can be quantitatively represented with the attenuation quality factor, Q (Kolsky, 1956; Futterman, 1962; White, 1965; Gladwin and Stacey, 1974; Kjartansson, 1979; Toksöz et al., 1979). Seismic signal processing techniques to recover the absorbed energy and velocity dispersion are called inverse Q filtering, which involves both model-based amplitude compensation and phase correction (Bickel and Natarajan, 1985; Hale, 1981, 1982; Gelius, 1987; Hargreaves and Calvert, 1991; Hargreaves, 1992; Bickel, 1993; Wang, 2002; Guo and Wang, 2004; Wang, 2006). We estimate the Q function directly from reflection seismic data (Wang, 2004), design stabilized inverse Q filters, and then apply them to 3-D seismic data (Figure 1b) with an attempt to improve the resolution for reservoir characterisation.

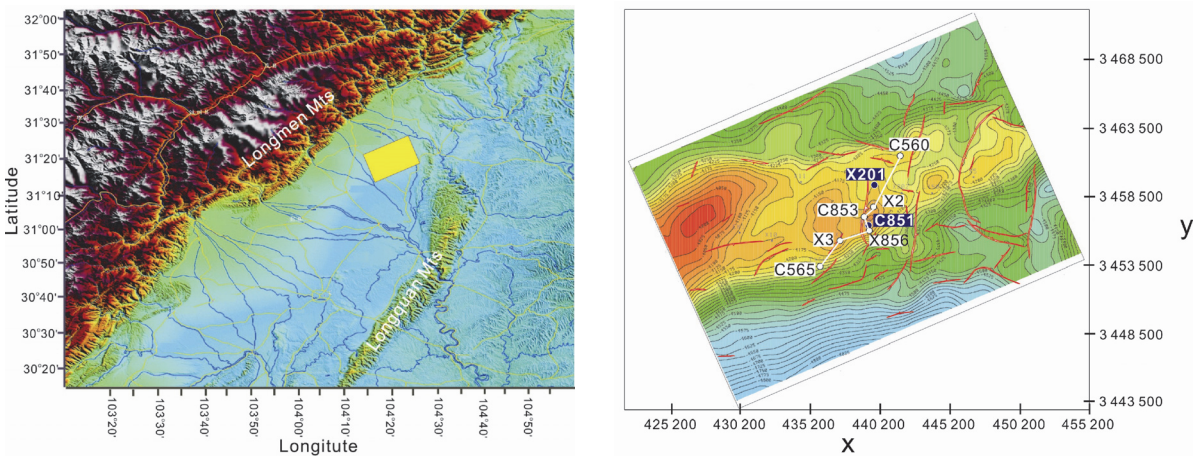

(*a*) (*b*)

Stratigraphy		Thickness (m)	Depth (m)	Gas stratum: Sand thickness (m)	Gas stratum: Porosity (%)	Section
J3	J3p	1200	600 800 1200	15 6 10	12.96	
	J3x	300		12	5	
J2	J2s	600	1800	20 13.5	6.1	
	J2x	200	2200	10	3.31	
	J2q	100				
J1	J1b	200	2600	5		
T3	$T3x^5$	400		5	7.53	
	$T3x^4$	600	3000	20 30		
	$T3x^3$	800	4000	15	4.4	
	$T3x^2$	500	4500	40 12	5 3.98	
	T3t	150				
	T3m	150				

(*c*)

Figure 1. (*a*) Location of study area (the yellow rectangle). (*b*) Base map of the 3-D seismic survey, corresponding to the yellow rectangular area. (*c*) Stratigraph of the Western Sichuan depression. Target gas reservoirs are in $T3x^2$ and $T3x^4$ of the Xujiahe Group, Upper Triassic continental clastic sediments.

The gas-sand thickness within production formations varies from 5 to 40 m, as indicated by red marks in Figure 1c. The low resolution of seismic data limits the ability to successfully explore the lateral extent of these sands. The stabilized inverse Q filtering technique simultaneously compensates the amplitudes and corrects for the phases, and may produce seismic cubes with enhanced resolution,

accurate timing, and improved signal-to-noise ratio (Wang, 2008). After the application of inverse *Q* filtering to the real seismic data, we see the following four advantages.

1) The seismic trace at a well location is well matched to the synthetic trace, due to the phase correction by inverse *Q* filtering.
2) Thin tight-sand layers are clearly presented in the seismic profile, due to the amplitude compensation of high frequency components.
3) Interesting low-amplitude zones corres-ponding to target high-fracture areas are clearly identified, due to the high signal-to-noise ratio of the stabilization scheme.
4) Finally, spatial variations of tight-sand layers are clearly depicted by the inversion profile due to its high resolution.

2. Tight-sand gas reservoirs

In the Western Sichuan depression, the surface exposed formation is from Quaternary of Cenozoic. Drilling reveals a normal stratigraphic sequence including Quaternary, Cretaceous, Jurassic and Triassic from the top downwards, as listed in Figure 1c, and the deepest formation encountered by drilling is the second member of the Xujiahe Group in the Upper Triassic, $T3x^2$, where T3 stands for the Upper Triassic, x stands for the Xijiahe Group, and the superscript indicates the member. Major gas reservoirs are the Penglai-zhen Group in the Upper Jurassic (J3p), the Shangshaxi-miao Group in the Middle Jurassic (J2s), and the Xujiahe Group in the Upper Triassic (T3x).

The target gas reservoirs in the Western Sichuan depression are in the Xujiahe Group, which consists of predominantly continental clastic sediments and can be divided into four members: $T3x^5$, $T3x^4$, $T3x^3$, and $T3x^2$, from shallow to deep stratigraphically. Among these four members, the major reservoirs are $T3x^4$ and $T3x^2$, which have a very small spatial variation in thickness. There is a variety of reservoir types including pores, fractures, fracture-plus-pores, and pore-plus-fractures. The reservoir type of $T3x^4$ is pores in the top and fracture-plus-pores in the bottom. The reservoir type of $T3x^2$ is fracture-plus-pores.

Laterally, the sedimentary environment in target reservoirs was relatively stable. Figure 1a is the structure map of the top of $T3x^2$. We can see that $T3x^2$ has a relatively small strata dip angle ($\leq 5°$) and undeveloped fractures. The general structure is relatively simple. However, because of very deep target reservoirs and a very thick near-surface low-velocity zone (from a few tens of metres to more than 200 metres), high-frequency components of a seismic signal decay very rapidly, and seismic reflections from target reservoirs have narrow bandwidths, low dominant frequencies (25–30 Hz), and a low resolution (1/4 wavelength > 45 m). Thus we cannot have adequate accuracy in the prediction of thin sand layers (with thickness < 20 m). One of the urgent projects in the current practice of deep gas reservoir exploration and production in Western Sichuan basin is how to enhance the resolution of deep-portion seismic data, so as to improve the prediction accuracy of potential reservoirs.

Vertically, Figure 2a compares the sand bodies at $T3x^4$ among six wells, which was linked by a white polyline in Figure 1b. It clearly shows the lateral distribution of sand bodies, and the sand development in the top, middle and bottom portions. As shown in Figure 2a, the top and bottom portions of $T3x^4$ have a very good sand development compared to the middle portion. The sand layers in both top and bottom portions may be easily identified from the logging information (Gamma-ray logs in the left and resistivity logs in the right) among different wells. $T3x^4$ sediment consists of 20 thin-layers of sand and sandstone gravel, with strong stratigraphic characteristics in the deposition cycle.

Figure 2b is a comparison of sand bodies among five wells at $T3x^2$. As displayed in Figure 2b, $T3x^2$ is the most sand-developed member within the Xujiahe Group, with very high sands-to-shale ratio (2–7). But because of less shale dissection, the deposition cycle characteristic in $T3x^2$ is not as

strong as that in T3x^4. In addition, there is very limited number of wells actually drilling through T3x^2, therefore it is difficult to identify thin-sand layers and to make lateral linkage unambiguously. Because the formation of T3x^2 has not been drilled through, it causes difficulty for the sand body comparison of the bottom part. It will also cause a problem for seismic inversion and reservoir characterisation, as there was no logging information in the deep part.

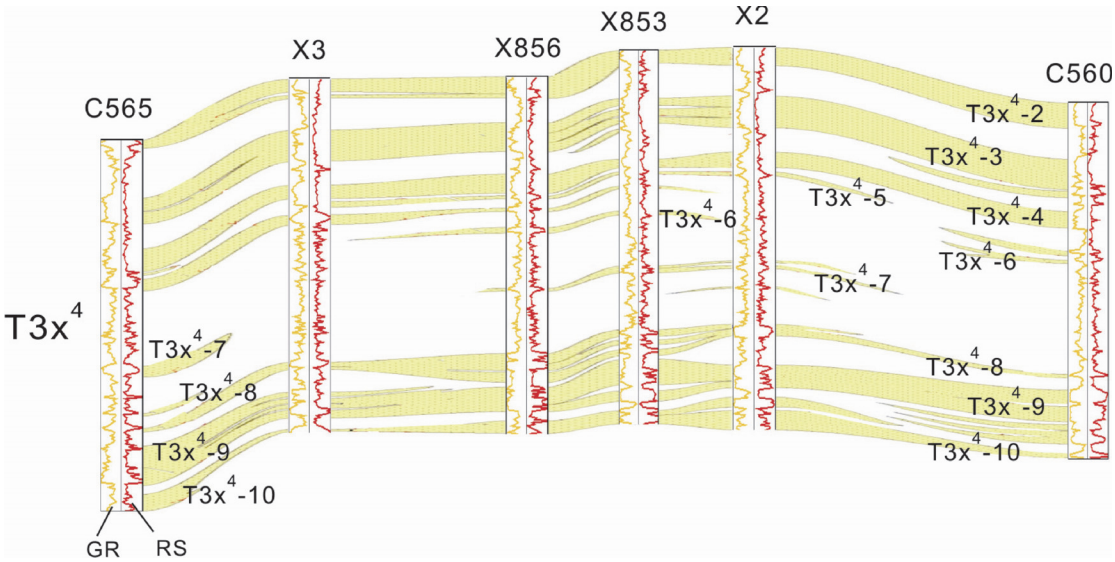

(*a*)

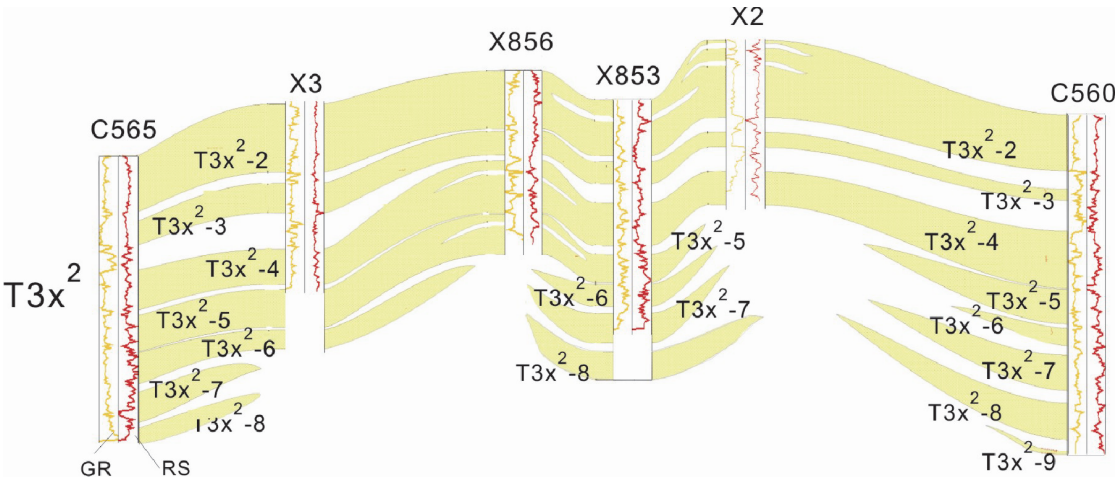

(*b*)

Figure 2. Sand distribution (yellow shade zones) within T3x^4 (*a*) and T3x^2 (*b*). Gamma-ray (GR) logs are in orange and resistivity (RS) logs are in red. Six wells are shown in Figure 1*b* and linked by a white line.

3. Stabilized inverse *Q* filtering

The inverse *Q* filtering algorithm we use here is a stabilized scheme, proposed by Wang (2002, 2006). For the completeness of the paper, we summarize the theory as follows.

Given a seismic trace $u(t)$, we can perform Fourier transform with respect to the time t, and present the seismic trace in the frequency domain as $U(\omega)$, where ω is the radial frequency. Inverse *Q* filtering is implemented as wavefield downward continuation on each frequency component separately. The wavefield $U(\tau = 0, \omega)$, recorded at the surface $\tau = 0$, is extrapolated down to the depth-time level τ. The extrapolated wavefield can be expressed as (Wang, 2002)

$$U(\tau,\omega)=U(0,\omega)\exp\left(\int_0^{\tau}\left(\frac{\omega}{\omega_{\mathrm{h}}}\right)^{-\gamma(\tau')}\frac{\omega}{2Q(\tau')}\mathrm{d}\tau'\right)\exp\left(\mathrm{i}\int_0^{\tau}\left(\frac{\omega}{\omega_{\mathrm{h}}}\right)^{-\gamma(\tau')}\omega\,\mathrm{d}\tau'\right), \tag{1}$$

where i is the imaginary unit, $Q(\tau)$ is a 1-D earth Q-model varying with traveltime, and $\gamma(\tau)=(\pi Q(\tau))^{-1}$. In expression (1), ω_{h} is related to the highest possible frequency in the exploration seismic frequency band (Wang and Guo, 2004), and is set as $2\pi\times100$ Hz in the following real data example.

The two exponential operators in equation (1) are amplitude compensation and phase correction terms. The latter is unconditionally stable, but the amplitude term needs to be stabilized (Wang, 2006). The stabilized inverse Q filtering formula is given as the following:

$$U(\tau,\omega)=U(0,\omega)\Lambda(\tau,\omega)\exp\left[\mathrm{i}\int_0^{\tau}\left(\frac{\omega}{\omega_{\mathrm{h}}}\right)^{-\gamma(\tau')}\omega\,\mathrm{d}\tau'\right], \tag{2}$$

where

$$\Lambda(\tau,\omega)=\frac{\beta(\tau,\omega)+\sigma^2}{\beta^2(\tau,\omega)+\sigma^2}, \tag{3}$$

$$\beta(\tau,\omega)=\exp\left(-\int_0^{\tau}\left(\frac{\omega}{\omega_{\mathrm{h}}}\right)^{-\gamma(\tau')}\frac{\omega}{2Q(\tau')}\mathrm{d}\tau'\right), \tag{4}$$

and σ^2 is the stabilization factor.

The time domain seismic signal, after inverse-Q filtering, is obtained by integrating all frequency-domain plane waves $U(\tau,\omega)$ at each time sample τ, as

$$U(\tau)=\frac{1}{\pi}\int_0^{\infty}U(0,\omega)\Lambda(\tau,\omega)\exp\left(\mathrm{i}\int_0^{\tau}\left(\frac{\omega}{\omega_h}\right)^{-\gamma(\tau')}\omega\,\mathrm{d}\tau'\right)\mathrm{d}\omega. \tag{5}$$

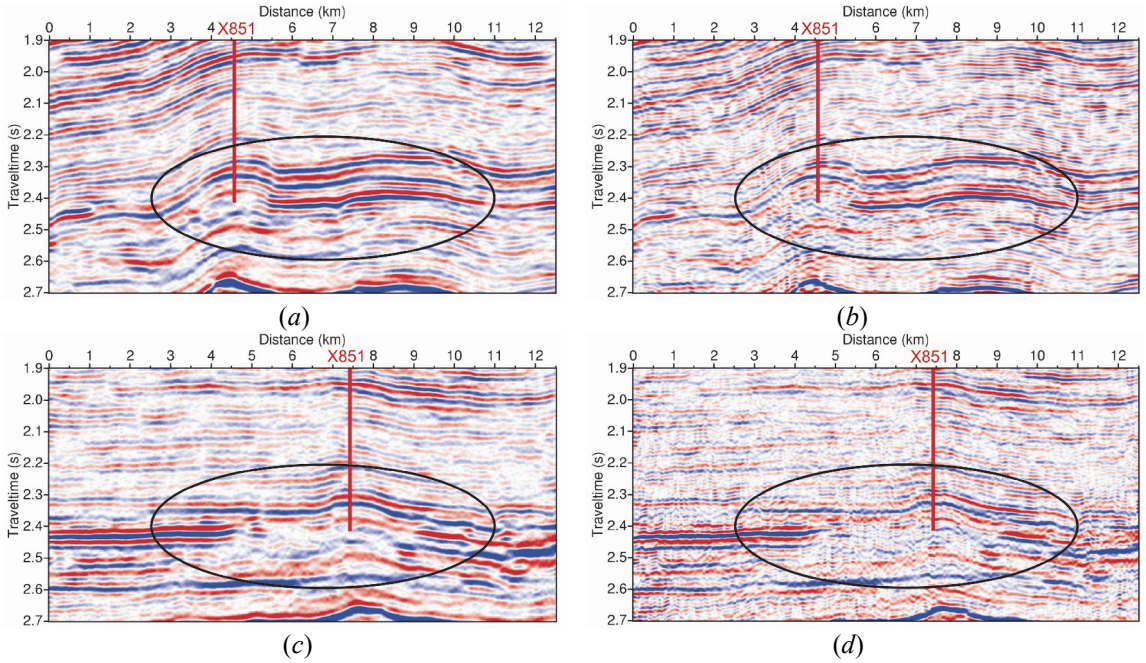

Figure 3. The inline (*a* and *b*) and the crossline (*c* and *d*) seismic sections before (*a* and *c*) and after (*b* and *d*) inverse Q filtering across a gas-producing well (X851).

We now apply this stabilized inverse Q filtering algorithm to a 3-D seismic data cube. Figures 3a and 3c display two seismic profiles before inverse-Q filtering. They are an inline section and a cross-line section, intersecting at a gas-production well X851. We can see that reflection wavelets in this original seismic section are lengthened gradually along with increased travel time, due to the attenuation of high-frequency plane waves. Inverse-Q filtering may compensate for the amplitude dissipation of plane waves and correct the phase distortion due to frequency dispersion. As shown in Figures 3b and 3d, the seismic sections after inverse-Q filtering show a great improvement in seismic resolution. After inverse-Q filtering, the width of reflected wavelets becomes consistent at all depths.

After inverse Q filtering, the improvement in resolution leads to the clear appearance of many subtle faults in the profile and detailed spatial variation in reflection layers. It reveals the variation in the thickness of the tight-sand gas reservoir at time 2.4 s near the production well. It indicates the clear existence of many small faults in different formation layers.

Figure 4 compares amplitude spectral curves before and after inverse Q filtering. It is evident that the dominant frequency is higher after inverse Q filtering, and the bandwidth is also wider than before inverse Q filtering. Most importantly, detailed features in the amplitude spectra between neighbouring frequencies, as indicated by ellipses, are kept unchanged after inverse Q filtering. This amplitude fidelity in the frequency domain is essential for any future exercise on fluid identification.

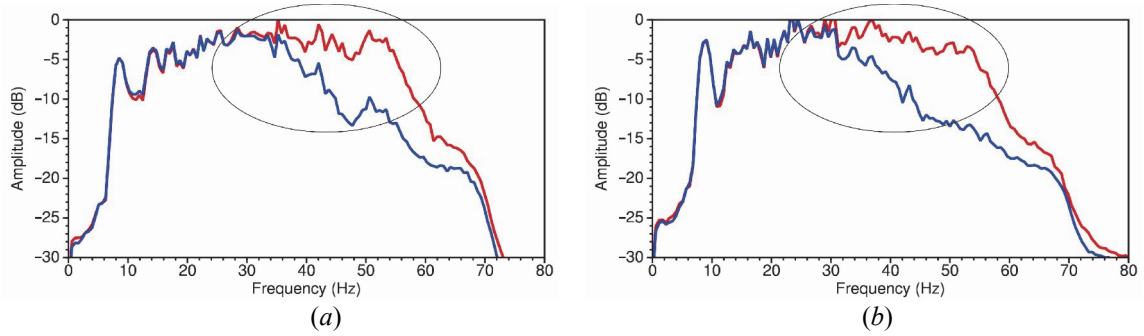

Figure 4. Seismic profile amplitude spectra of the inline (*a*) and crossline (*b*) seismic profiles before (blue) and after (red) inverse Q filtering.

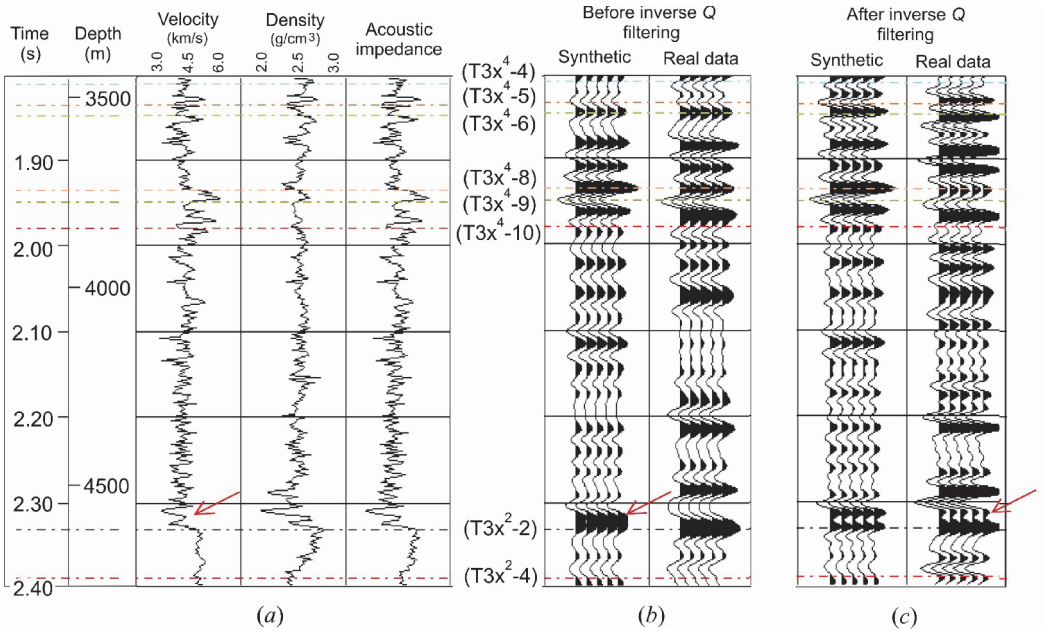

Figure 5. Comparison of synthetic and real seismic traces (at well X851) before and after inverse Q filtering. (*a*) Velocity, density and acoustic impedance curves. (*b*) Synthetic and real seismic traces before inverse Q filtering. (*c*) Synthetic and real seismic traces after inverse Q filtering. Each of synthetic and real seismic traces is plotted 5 times.

4. Reservoir identification

4.1 Identify thin-layer interbeds

Figure 5 displays comparison of seismic traces before and after inverse *Q* filtering, at Well X851. Figure 5a plots velocity, density and acoustic impedance at Well X851. From the well-log information, we can see that at the top of the T3x^2-2 sand body, there is a set of interbedded low-velocity shales and thin sandstones. Before inverse *Q* filtering, as shown in Figure 5b, it appears as a composite reflection wave, both on the real seismic trace at the well location and on the synthetic generated from convolution of the reflectivity series calculated from well logging and a wavelet extracted from the seismic trace. After inverse *Q* filtering, as shown in Figure 5c, above the strong reflection at the top of T3x^2-2 sand body, there is a new reflection. Synthetic calibration further verifies that this new reflection is a reliable reflection from the interbedded low-velocity shale and thin sandstones.

Figure 6 compares the synthetic trace at Well X851 with a small portion of seismic profiles around. Each synthetic trace (in red) is plotted 5 times to facilitate the comparison. This time, the wavelet used for synthetic traces (red traces) is a zero-phase Ricker wavelet. The dominant frequency of the Ricker wavelet is 30 Hz (left) and 35 Hz (right) for the comparison with seismic sections before and after inverse *Q* filtering, respectively. From the Gamma ray log in Figure 6 we can see that the bottom of T3x^3, immediately above the top of T3x^2-2, is a set of shale with a high Gamma value. At its bottom, there is a relatively high-velocity thin layer (indicated by arrows) interbedded within such a set of shale with a remarkably low velocity. Both synthetics using 30 and 35 Hz wavelets, respectively, appear as a dual-peak reflection. Such a dual-peak reflection characteristic can be used to clearly identify thin layer interbeds. Typically, on an inverse *Q* filtered seismic profile, the reflection from the thin layer interbed can be well identified, but cannot be identified in the seismic profile before inverse *Q* filtering.

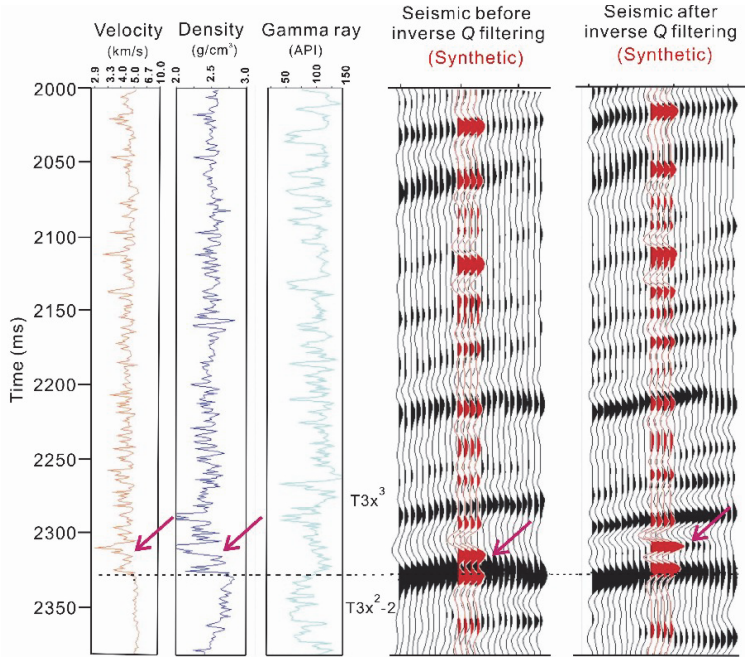

Figure 6. Comparison of synthetic traces at well X851 with real seismic sections before and after inverse *Q* filtering. Each synthetic trace (in red) is plotted 5 times to facilitate the comparison with seismic sections.

Comparison of synthetics and real seismic sections shows that the inverse *Q* filtered seismic section has a better correlation with synthetic traces. After inverse *Q* filtering, not only has the resolution been enhanced, but also the phase has been corrected. In general, the waveform appears

more zero-phase-like. Reservoir identification further testifies the reliability of the inverse *Q* filtering scheme.

4.2 Anomalous amplitude 'dim' spots

Dim spots are a type of local seismic event that, in contrast to a bright spot, shows weak rather than strong amplitude. The weak amplitude might correlate with hydrocarbons that reduce the contrast in acoustic impedance between the reservoir and the overlying rock, or might be related to a stratigraphic change that reduces acoustic impedance.

Exploration experiences suggest that the $T3x^2$ gas reservoir has very strong spatial heterogeneity both horizontally and vertically. The 'efficient fluid penetrating zone' built by fracture networks within high-quality reservoirs with relatively high porosity is the essential factor for high and steady production. In a seismic section, as shown in Figure 7a, the seismic response of the so-called efficient fluid-penetrating zones appear as the anomalous dim spots (inside yellow dotted circles) with characteristic 'strong-events terminated and weak-reflections cluttered'. After inverse *Q* filtering which enhances the resolution of the seismic profile (Figure 7b), the characteristics of seismic dim spots are still preserved Moreover, the internal reflection structure within the efficient fluid penetrating zone becomes much clearer, as the signal-to-noise ratio has been improved remarkably.

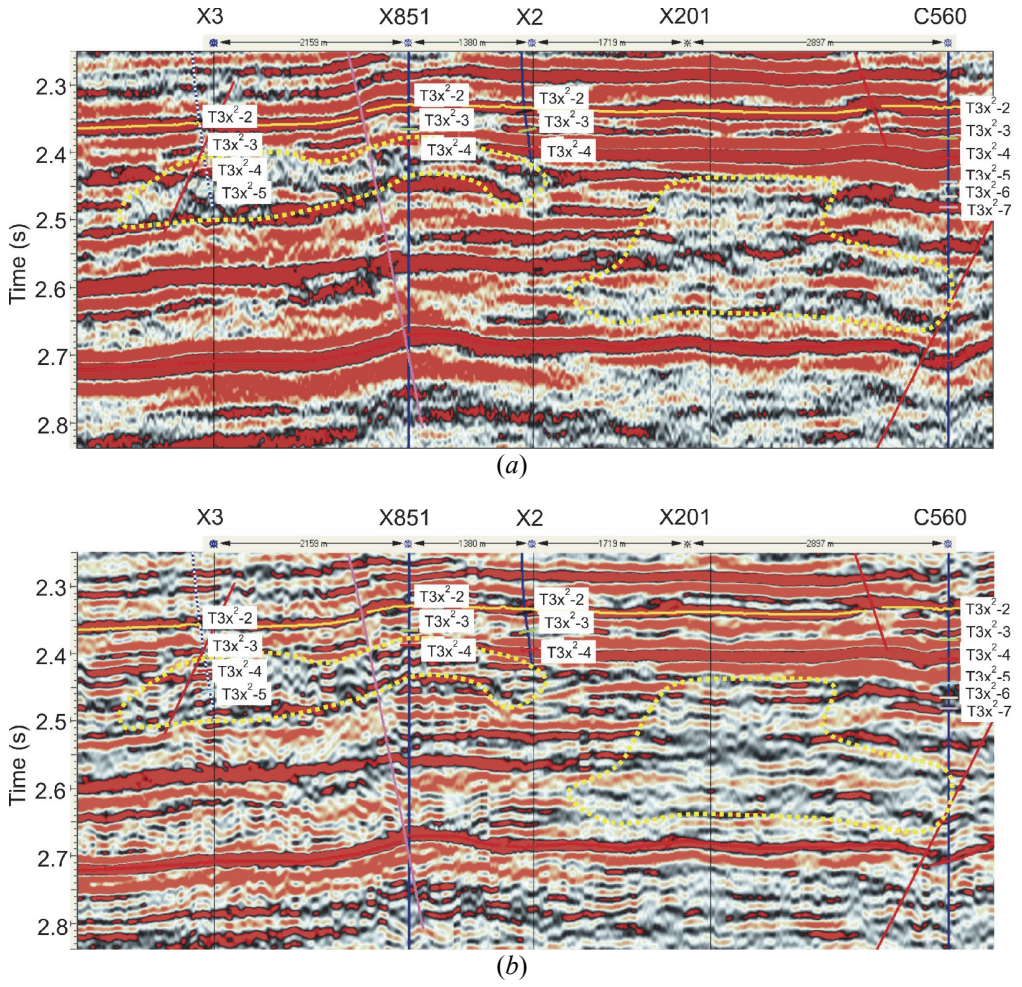

Figure 7. Seismic responses of the so-called 'efficient penetrating zone'. (*a*) Seismic section before inverse *Q* filtering. (*b*) Seismic section after inverse *Q* filtering. The clear anomalous amplitude 'dim spots' are still preserved, but the signal-to-noise ratio within the zone has been improved after inverse *Q* filtering.

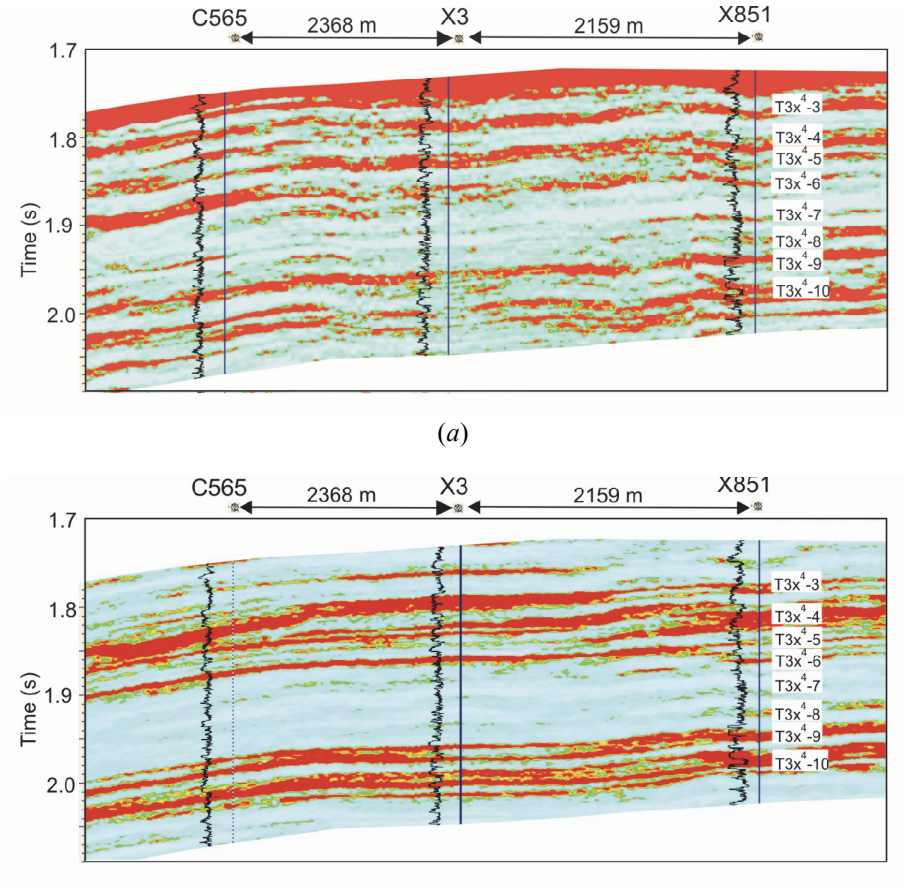

Figure 8. Seismic inversion and reservoir characterisation of $T3x^4$, based on seismic data before (*a*) and after (*b*) inverse *Q* filtering. Gamma-ray logs are used as constraints in seismic stochastic inversion. Lateral continuation of tight-sand reservoirs can be much more clearly tracked in the inversion result of seismic data after inverse *Q* filtering.

4.3 Seismic inversion and characterization

For the tight clastic sediments within the Xujiahe Group in Western Sichuan, Gamma-ray logging is the most effective piece of information to identify sand bodies. Thus, we use Gamma ray logs as a constraint to perform stochastic inversion and sand lateral description. Figure 8 compares two inversion results, based on seismic data before and after inverse *Q* filtering. The positions of well-logs can be found in Figure 1b. In Figure 8b, based on inverse-*Q* filtered high-resolution seismic data, the lateral extent of most sandstone layers within $T3x^4$ can be much more clearly tracked than that in Figure 8a obtained from seismic data without inverse *Q* filtering. For instance, the last two members, $T3x^4$-9 and $T3x^4$-10, show not only a strong lateral continuity but also a clear spatial variation.

Therefore, high-resolution seismic data produce high-resolution inversion results with an adequate accuracy for the prediction of sand reservoirs in the study area. However, because the deep $T3x^2$ has a lack of well-logging information, we cannot obtain a reliable inversion result as accurate as $T3x^4$.

5. Conclusions

This paper demonstrates the application of inverse *Q* filtering to successfully enhance the resolution of 3-D seismic data, for the characterisation of tight-sand gas reservoirs. After inverse *Q* filtering, the frequency bandwidth has been increased by about 10 Hz, and the width of the wavelet has been narrowed, so that we are able to identify reflections of thin sand layers clearly. The character of

relative strength of neighbouring frequencies has remained unchanged, which indicates the high fidelity of the algorithm. As signal-to-noise ratio has been improved, reservoir identification becomes easier, anomalous amplitude dim spots are clearer, and the detail within the anomalies can also be seen. Finally, we are able to use inverse-*Q* filtered seismic data in seismic inversion, to generate a high-resolution image for sand-body characterisation.

Acknowledgments

We are grateful to the sponsors of the Centre for Reservoir Geophysics, Imperial College, for supporting this research, and to the Southwest Petroleum Company of Sinopec for permission to publish this work.

References

Bickel S H 1993 Similarity and the inverse *Q* filter: the Pareto-Levy stretch *Geophysics* **58** 1629–33
Bickel S H and Natarajan R R 1985 Plane-wave *Q* deconvolution *Geophysics* **50** 1426–39
Futterman W I 1962 Dispersive body waves *J. Geophys. Res.* **67** 5279–91
Gelius L J 1987 Inverse *Q* filtering: a spectral balancing technique *Geophys. Prospect.* **35** 656–67
Gladwin M T and Stacey F D 1974 Anelastic degradation of acoustic pulses in rock *Phys. Earth Planet. Inter.* **8** 332–6
Guo J and Wang Y 2004 Recovery of a target reflection underneath coal seams *J. Geophys. Eng.* **1** 46–50
Hale D 1981 An inverse-*Q* filter *Stanford Exploration Project Report* No 26 231–43
Hale D 1982 *Q*-adaptive deconvolution *Stanford Exploration Project Report* No 30 133–58
Hargreaves N D 1992 Similarity and inverse *Q* filter: some simple algorithms for inverse *Q* filtering *Geophysics* **57** 944–7
Hargreaves N D and Calvert A J 1991 Inverse *Q* filtering by Fourier transform *Geophysics* **56** 519–27
Kjartansson E 1979 Constant *Q* wave propagation and attenuation *J. Geophys. Res.* **84** 4737–48
Kolsky H 1956 The propagation of stress pulses in viscoelastic solids *Phil. Mag.* **1** 693–710
Tang J, Zhang S and Li X 2008 PP and PS seismic response from fractured tight gas reservoirs: a case study *J. Geophys. Eng.* **5** 92–102
Toksöz M N, Johnston D H and Timur A 1979 Attenuation of seismic waves in dry and saturated rocks, I: laboratory measurements *Geophysics* **44** 681–90
Wang Y 2002 A stable and efficient approach to inverse *Q* filtering *Geophysics* **67** 657–63
Wang Y 2004 *Q* analysis on reflection seismic data *Geophys. Res. Lett.* **31** L17606
Wang Y 2006 Inverse *Q* filtering for seismic resolution enhancement *Geophysics* **71** V51–60
Wang Y 2008 *Seismic Inverse Q Filtering* (Oxford: Blackwell)
Wang Y and Guo J 2004 Modified Kolsky model for seismic attenuation and dispersion *J. Geophys. Eng.* **1** 187–96
White J E 1965 *Seismic Waves: Radiation, Transmission and Attenuation* (New York: McGraw-Hill)